SPANDIDOS PUBLICATIONS

ONCOLOGY REPORTS 49: 20, 2023

Progress of radiological-pathological workflows in the differential diagnosis between primary central nervous system lymphoma and high-grade glioma (Review)

LUMING CAO[1*], MENGCHAO ZHANG[2*], YING ZHANG[1*], BIN JI[3], XUEMEI WANG[1] and XUEJU WANG[1]

Departments of [1]Pathology, [2]Radiology and [3]Nuclear Medicine, China-Japan Union Hospital, Jilin University, Changchun, Jilin 130033, P.R. China

Received June 24, 2022; Accepted November 3, 2022

DOI: 10.3892/or.2022.8457

Abstract. Primary central nervous system lymphoma (PCNSL) and high-grade glioma (HGG) are distinct entities of the CNS with completely distinct treatments. The treatment of PCNSL is chemotherapy-based, while surgery is the first choice for HGG. However, the clinical features of the two entities often overlap, and a clear pathological diagnosis is important for subsequent management, especially for the management of PCNSL. Stereotactic biopsy is recognized as one of the minimally invasive alternatives for evaluating the involvement of the CNS. However, in the case of limited tissue materials, the differential diagnosis between the two entities is still difficult. In addition, some patients are too ill to tolerate a needle biopsy. Therefore, combining imaging, histopathology and laboratory examinations is essential in order to make a clear diagnosis as soon as possible. The present study reviews the progress of comparative research on both imaging and laboratory tests based on the pathophysiological changes of the two entities, and proposes an integrative and optimized diagnostic process, with the purpose of building a better understanding for neurologists, hematologists, radiologists and pathologists.

Contents

Correspondence to: Dr Xueju Wang, Department of Pathology, China-Japan Union Hospital, Jilin University, 126 Xiantai Street, Changchun, Jilin 130033, P.R. China
E-mail: xueju@jlu.edu.cn

[*]Contributed equally

Key words: primary central nervous system lymphoma, high-grade glioma, pathology, radiology, diagnostic workflow

1. Introduction

Primary central nervous system lymphoma (PCNSL) and high-grade glioma (HGG) are malignant brain tumors, with annual incidence rates of ~0.45 and 4 per 100,000 population, respectively, in the United State (1). The diseases can mimic each other in clinical, radiological and even pathological examinations (2,3); however, they require completely different management. Approximately 90% of PCNSL cases are diffuse large B-cell lymphomas (DLBCL). High-dose methotrexate-based polychemotherapy plus rituximab is currently the treatment of choice for CNS DLBCL (4). Conversely, the primary treatment modality for HGG is surgery, followed by chemotherapy and radiotherapy (5). Furthermore, prior to surgery, corticosteroids can be administered to decrease the symptomatic tumor-associated edema of HGG. As the management is completely different for these entities, a precise diagnosis is crucial.

PCNSL and HGG can display overlapping clinical, radiological and partial pathological features that cause challenges in making the differential diagnosis between them. Firstly, both entities show a predilection for males and older patients (>65 years old) (1), commonly involving the deep white matter and the corpus callosum (6,7). The symptoms are associated with the involved areas of the brain, such as focal neurological deficits, neurocognitive impairment, seizures and signs of elevated intracranial pressure (headaches, nausea and vomiting) (6,8). Secondly, PCNSL and glioblastoma multiforme (GBM) can mimic each other in both imaging and histological examinations. For example, a case report (9) showed that CNS DLBCL in an immunocompromised patient was misdiagnosed as GBM by ring-like enhancement on contrast-enhanced T1-weighted imaging (CE-T1WI) and obvious edema in T2-fluid-attenuated inversion recovery (T2-FLAIR) images. This case was also misdiagnosed as GBM on intraoperative frozen section examination showing coagulation necrosis and atypical cell infiltration. DLBCL

was recorded as the final diagnosis until postoperative formalin-fixed, paraffin-embedded (FFPE) tissue examination accompanied by immunohistochemistry (IHC) staining was performed. Similarly, another case report (10) mentioned that GBM was also nearly misdiagnosed as CNS DLBCL on magnetic resonance imaging (MRI) with and without gadolinium-based contrast, which showed little surrounding edema and mild diffusion restriction. Flow cytometry of the cerebrospinal fluid (CSF) also revealed an abnormal B-cell population, providing further evidence for the diagnosis of lymphoma. However, a stereotactic biopsy of the brain mass confirmed the diagnosis of GBM.

Pathological changes in FFPE tissues accompanied by IHC staining are acknowledged as the gold standard for the diagnosis of brain tumors. Microscopically, PCNSL typically exhibits high cellularity and a diffuse growth pattern. Large central areas of geographical necrosis are usually accompanied by variable to frequent perivascular lymphoma islands from central to peripheral lesions. Astrocytic and microglial proliferation, as well as inflammatory reactions, are often observed in the surrounding parenchyma. GBM also presents with large central necrotic areas surrounded by accumulated pleomorphic glial tumor cells in the periphery. Compared with PCNSL, HGG displays microvascular proliferation, which is usually most marked around necrotic foci and in the peripheral zone of infiltration. In some cases, there are isolated tumor cells or islands infiltrating the parenchyma rather than distinct masses, or the tumor cells show obvious heterogeneity, especially in stereotaxic needle biopsies; thus, further IHC staining is needed to make a differential diagnosis (11).

Stereotactic biopsy is sometimes inconclusive after the use of corticosteroids, which can induce rapid tumor shrinkage and false-negative results (12), especially with limited specimens. In one study, the rate of occurrence of false-negative biopsies after <1 week of steroid treatment was 33.3%, increasing to 57.1% after >1 week of steroid treatment (2). A reasonable interval of at least 2-4 weeks after withholding steroid usage is recognized as necessary prior to brain biopsy (2,13-15), yet this causes a delay in the diagnosis of PCNSL. Furthermore, stereotactic biopsy is not always feasible in patients (13). Thus, imaging, liquid analysis and molecular tests are quite meaningful for prompt diagnosis and can provide circumstantial evidence for pathological examinations, especially with limited samples. Although independent diagnostic research progress for PCNSL and HGG is abundant, the present narrative review only includes the progress from comparative diagnostic studies between PCNSL and HGG, with the purpose of building a liaison between radiology and pathology, as well as to provide more options for clinicians to improve the accuracy and speed of the decision-making process.

2. Radiological progress in PCNSL and HGG

Conventional MRI. According to the National Comprehensive Cancer Network guidelines (16), MRI with and without contrast serves as the first-line recommendation for the differentiation of PCNSL and HGG. CNS DLBCL typically presents as iso- to hypointense on unenhanced T1-weighted MRI (17), as iso- to hyperintense on T2-weighted imaging (T2WI) and as homogeneous enhancement on CE-T1WI (4). By contrast, HGG usually presents with central hypointensity similar to CSF and a marginal slightly high signal on T2WI, and as a heterogeneous, ring-enhancing lesion (5). Edema around the HGG lesion can be clearly observed on the T2-FLAIR sequence. As aforementioned, signal changes in these conventional MR sequences can often reflect some histological information, such as edema, hemorrhage and necrosis. However, there are considerable overlapping appearances between PCNSL and HGG in atypical cases, which cause confusion in conventional MRI, especially in cases of immunodeficiency and after treatment. For example, GBM with homogeneous enhancement but no apparent necrosis may mimic PCNSL, while atypical PCNSL with heterogeneous enhancement and central necrosis may mimic GBM (18). However, advanced MRI techniques can provide more evidence for the differential diagnosis.

Cellularity and diffusion-weighted imaging (DWI). DWI calculates the apparent diffusion coefficient (ADC) values to quantify the diffusion of unbound extracellular water molecules (19). Differences in cellularity between PCNSL and GBM can be assessed using DWI. High cellular density and a large nuclear to cytoplasmic ratio lead to the reduction of water diffusion (19), which causes increased signal shadows and a decreased ADC value (20), differentiating untreated PCNSL from GBM (21-24). Different ADC parameters have been discussed for the purpose of differential diagnosis, including ADC_{min}, $rADC_{mean}$, and $ADC_{5\%}$ [the lowest and mean ADC value obtained from placed regions of interest was defined as the minimum ADC (ADC_{min}) and mean ADC (ADC_{mean}), respectively. $rADC_{mean}$=(ADC_{mean} of the tumor)/(ADC_{mean} of the normal appearing white matter of the contralateral hemisphere). Percentile values are the Nth percentile from the ADC histograms that reflect the distribution of ADC values in the region of interest. $ADC_{5\%}$ is the fifth percentile from the ADC histograms that reflect the distribution of ADC values in the region of interest]. All ADC parameters are lower in PCNSL compared with those in GBM. A previous study (25) demonstrated a cutoff value of 0.68×10^{-3} mm^2/sec for $ADC_{5\%}$ to differentiate CNS DLBCL and GBM, with a sensitivity of 100%. In addition, molecular types of tumors may affect ADC values. For example, MYC proto-oncogene bHLH transcription factor (MYC) and BCL2 apoptosis regulator (BCL2) gene rearrangements in CNS DLBCL lead to lower $rADC_{min}$ and $rADC_{mean}$ values, while isocitrate dehydrogenase [NADP(+)]1 (IDH1) mutation in GBM leads to higher values, when compared with wild-types (18). Methylation of the O(6)-methylguanine-DNA methyltransferase (MGMT) promoter in GBM may lead to higher ADC values with lower perfusion (26). Epidermal growth factor receptor variant III mutant GBM showed a higher cell density, leading to increased perfusion and a lower ADC value (27).

Combined conventional MRI and DWI can more accurately reflect histologically related information for the differential diagnosis. Fig. 1 presents representative combined images from the Department of Radiology of China-Japan Union Hospital of Jilin University (Changchun, China). For example, typical images of a representative DLBCL case occurring in the left temporal lobe are shown in Fig. 1. The lesions were classified as isointense on T1WI and T2WI, as high intensity on FLAIR, surrounded by finger-like edema limited

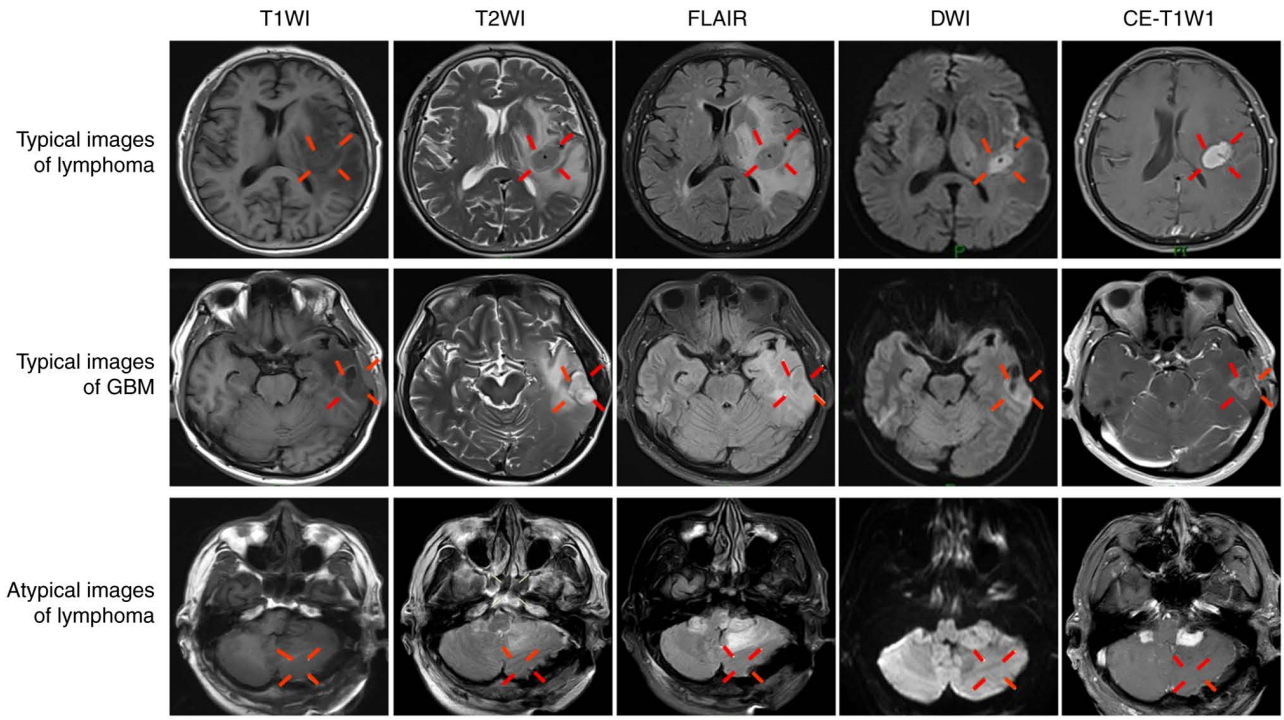

Figure 1. Original magnetic resonance imaging of central nervous system lymphoma or high-grade glioma. Typical images of DLBCL are shown in the top row. The lesion displays as isointense on T1WI and T2WI, as high intensity on FLAIR surrounded by finger-like edema, with limited diffusion on DWI, and with uniform and obvious enhancement on CE-T1W1. Typical images of GBM lesions are shown in the middle row. The lesion displays a low signal on T1WI, a high signal surrounded by finger-like edema on T2WI, as isointense on FLAIR, with no restricted diffusion on DWI, and as garland-like enhancement on CE-T1W1. Atypical images of multiple DLBCL neoplastic lesions are shown in the bottom row. The lesions display as isointense on T1WI and T2WI, as slightly hyperintense on FLAIR with no surrounding edema, with no restricted diffusion on DWI and with obvious uniform enhancement on CE-T1WI. Red lines surround and indicate the lesion in each image. DLBCL, diffuse large B-cell lymphoma; CE-T1WI, contrast-enhanced T1-weighted imaging; FLAIR, fluid-attenuated inversion recovery; DWI, diffusion-weighted imaging; GBM, glioblastoma.

diffusion on DWI, and as uniform with obvious enhancement on CE-T1W1. Representative images from a GBM case are also shown in Fig. 1. The lesions occurred in the left temporal lobe, with a low signal on T1WI and a high signal surrounded by finger-like edema on T2WI. The lesions were isointense on FLAIR, and showed restricted diffusion on DWI and garland-like enhancement on CE-T1W1. However, lymphoma often presents with atypical images, not only in conventional MRI, but also in DWI. Fig. 1 shows a representative case in which the lesions, which occurred in the posterior fossa and were finally diagnosed as DLBCL by pathological examination, presented as isointense on T1WI and T2WI, as slightly hyperintense on FLAIR, with no surrounding edema and no restricted diffusion on DWI, and as obvious uniform enhancement on CE-T1WI. Thus, more parameters were needed for the differential diagnosis.

Angiogenesis and dynamic susceptibility contrast (DSC) MRI. DSC MRI is perfusion MRI using contrast medium injection. DSC MRI tracks the T2 weighted signal to the image and calculates perfusion metrics (28). Differences in angiogenesis between PCNSL and HGG can be reflected by cerebral blood flow (CBF) and cerebral blood volume (CBV). Compared with HGG, PCNSL displays lower CBF and CBV values due to the absence of neovascularization (29). Neska-Matuszewska *et al* (30) reported that max rCBV [max rCBV=(CBV_{max} of the tumor)/(CBV_{max} of the normal appearing white matter of the contralateral hemisphere)] demonstrated a high accuracy of 98.5% in differentiating 16 CNS B-cell lymphomas from 20 GBMs and 20 metastases. Arterial spin labeling (ASL) can be used to detect CBF values by non-invasively labeling blood without injection of contrast medium (31). It is suitable for patients who cannot undergo the injection of a contrast agent. A meta-analysis showed that DSC had a higher diagnostic accuracy than ASL in differentiating HGG from PCNSL (31). However, the accuracy of CBV decreases due to damage to the blood-brain barrier (BBB) from both HGG and PCNSL, which causes contrast agent leakage (32). A preload contrast dose is used to minimize the effects of leakage (19). After a preload injection, Chaganti *et al* (33) used a mean rCBV of 2.68 to differentiate 11 PCNSLs from 15 HGGs, with an area under the curve (AUC) of 1.000.

BBB damage and DSC or dynamic contrast-enhanced (DCE) MRI. Serious BBB damage can be analyzed by percentage signal recovery (PSR) and volume transfer constant (K^{trans}), which can compensate for the deficiency of CBV. In the study by Cindil *et al* (32), both parameters were reported to be higher in PCNSL than in HGG. The PSR was calculated from the time-signal curve of DSC MRI. PSR represents a complex combination of tissue microstructure and hemodynamic effects, such as blood flow, vascular permeability and cellular geometry (34). PSR is a promising parameter that performs better than rCBV in both a PSR-optimized protocol without preload (AUC, 0.979) (32) and a CBV-optimized protocol with preload (AUC, 0.830) (35). K^{trans} is a parameter of permeability

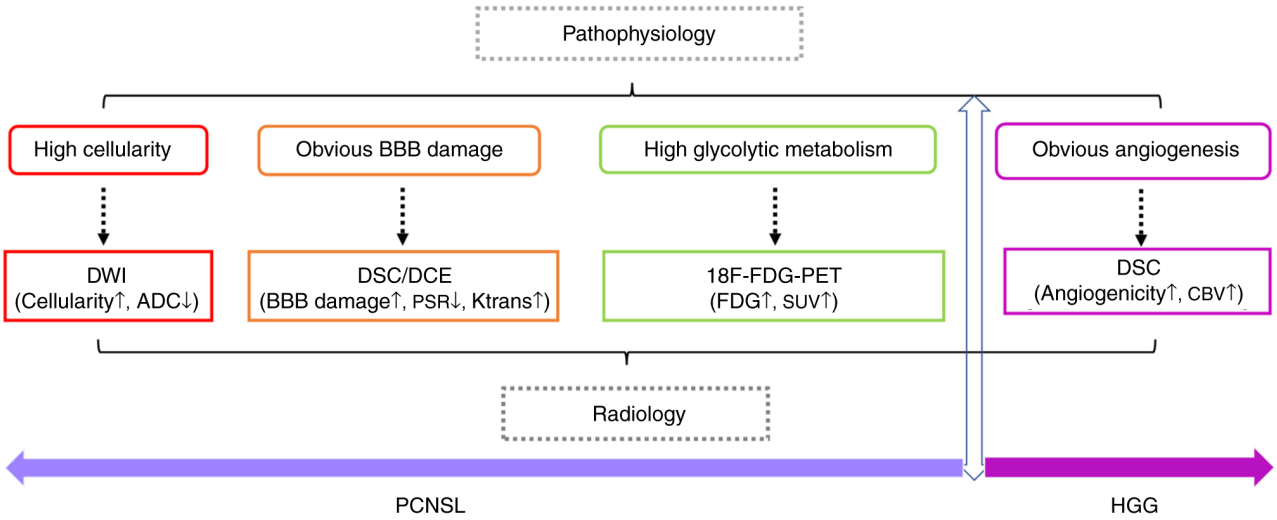

Figure 2. Association between pathology and radiology in the differential diagnosis of PCNSL and HGG. PCNSL shows high cellularity, a diffuse growth pattern and BBB damage, and a high glycolytic metabolism, which correspond to low ADC values in DWI, increased PSR values in DSC MRI, increased K^{trans} values in DCE MRI and high FDG uptake on PET/CT. By contrast, obvious angiogenesis of HGG can be reflected by an increased CBV value in DSC MRI. HGG, high-grade glioma; PCNSL, primary central nervous system lymphoma; BBB, blood-brain barrier; ADC, apparent diffusion coefficient; DWI, diffusion-weighted imaging; PSR, percentage signal recovery; K^{trans}, volume transfer constant; MRI, magnetic resonance imaging; DSC, dynamic susceptibility contrast; DCE, dynamic contrast-enhanced; FDG, [18F] fluorodeoxyglucose; PET/CT, positron emission tomography/computed tomography; CBV, cerebral blood volume.

calculated from T1-weighted signal curves and is obtained from DCE MRI (28). It is still controversial to evaluate the effect of the K^{trans} parameter for the differentiation between PCNSL and HGG. One previous study (21) reported no significant difference in the distribution of K^{trans} between CNS DLBCL and GBM. However, another study by Lu *et al* (22) revealed that a cutoff of 0.187 for K^{trans} reached a high AUC of 0.852 for differentiating CNS DLBCL from GBM.

Microhemorrhage, calcification and neovascularity, and susceptibility-weighted imaging (SWI). Differences in microhemorrhage, calcification and neovascularity (veins) between CNS DLBCL and GBM could be reflected by the intratumoral susceptibility signal (ITSS) on SWI (36). A higher ITSS presents more dot-like foci of susceptibility within the tumor. In one study, the ITSS was significantly higher in GBM than in B-cell PCNSL, and performed well in the differentiation of PCNSL from GBM, with an AUC of 0.800 (37). In addition, a recent study (18) reported lower ITSS and higher rSWI values [rSWI=(mean SWI of the tumor)/(mean SWI of the matching contralateral normal-appearing white matter)] in IDH1-mutant GBM compared with those in wild-type GBM, suggesting that it would be difficult to distinguish B-cell type PCNSL from IDH1-mutant GBM by ITSS or mean rSWI value.

Metabolism and MR spectroscopy (MRS) or positron emission tomography (PET)/computed tomography (CT). The alterations in metabolites such as lipid and myo-inositol (mIns) within the tumor could be detected by MRS. Lipid levels are associated with necrosis and the activation of lymphocytes and macrophages, which are significantly higher in PCNSL than in GBM (8,38). The mIns level reflects the expression of inositol-3-phosphate synthase 1 (ISYNA1), which is the rate-limiting enzyme of the first step in the biosynthesis of mIns. Higher ISYNA1 expression in GBM leads to a higher mIns level (39).

Different uptake of radiotracers between PCNSL and HGG is presented by the tumor to normal contralateral cortex activity (T/N) ratio and standardized uptake value (SUV). The SUV and T/N ratio are semiquantitative indicators of radiotracer utilization. Most clinical centers use a radiolabeled glucose analog such as [18F] fluorodeoxyglucose (FDG) as the tracer (19). Other tracers such as 11C-methionine also show potential value in differentiating PCNSL from GBM; however, 11C-methionine has limited value in the clinical routine due to its short half-life (20 min) (40). The SUV of FDG is significantly higher in CNS lymphoma than in GBM due to the higher tumor cell density with elevated glycolytic metabolism (41). Nakajima *et al* (25) reported that a cutoff SUV_{max} value of 9.35 performed well in differentiating CNS DLBCL from GBM, with an AUC of 0.933. Similarly, Zhou *et al* (42) reported an AUC of 0.910 for differentiating 40 PCNSLs from 52 GBMs, with a higher SUV_{max} cutoff value of 13.77. However, some atypical PCNSLs show low FDG uptake, which is closely associated with the negative expression of mutated melanoma-associated antigen 1 protein (43).

Preferred radiology workflow for the differential diagnosis of PCNSL from HGG. Details of all radiological parameters and case numbers of PCNSL and GBM involved in a series of studies are summarized in Table SI. Marked differences between PCNSL and HGG were observed in DWI, DSC/DCE and 18F-FDG-PET/CT, which corresponded to the pathophysiological features of the two entities. As shown in Fig. 2, PCNSL presents with a diffuse growth pattern, obvious BBB damage and high cellularity associated with elevated glycolytic metabolism, which correspond to low ADC values in DWI, increased PSR values in DSC MRI, increased K^{trans} values in DCE MRI and high FDG uptake on PET/CT. Furthermore, the feature of microvascular proliferation of HGG can be reflected by an increased CBV value in DSC.

3. Progress of radiomics and machine learning

Radiomics analyses provide promising evidence for a differential diagnosis, especially in tumors with high heterogeneity (44). Radiomics includes feature-based and deep learning-based components. Feature-based radiomics uses a series of mathematically predefined features that are typically extracted from a segmented region (45). Deep learning-based radiomics utilizes artificial neural networks that imitate the vision of humans and automatically extract high-dimensional features from the input images at different levels of scaling and abstraction (45).

Feature-based radiomics. The diagnostic value of image features extracted from different MRI types was researched for feature-based radiomics. Priya *et al* (46) found that features extracted from CE-T1WI could distinguish between 46 PCNSLs and 97 GBMs, with an AUC of 0.924. Different combinations of conventional MRI such as T1WI, T2WI, CE-T1WI and FLAIR also performed well using feature-based radiomics (47-49). MacIver *et al* (50) reported the high performance of an ADC map for diagnosing 48 PCNSLs and 42 GBMs (AUC, 0.880). Mehrnahad *et al* (51) also concluded the usefulness of feature-based radiomics derived from an ADC map in differentiating 57 GBMs from 25 PCNSLs. The diffusion condition of tumors in the ADC map was combined with CE-T1WI and analyzed by feature-based radiomics. The combination was as effective as radiologists, with an AUC of 0.946 when differentiating 14 PCNSLs from 28 GBMs (52). In one study, a radiomics model combining CE-T1WI and ADC maps (AUC, 0.935) performed better than veteran radiologists (AUC, 0.923-0.945) for distinguishing between 26 PCNSLs and 22 GBMs (53). Kim *et al* (54) used multi-parametric MRI (T2WI, CE-T1WI and ADC) for differentiating PCNSL and GBM, with an AUC of 0.956. Combining CE-T1WI, ADC and FLAIR also showed high accuracy (AUC, 0.977) (55). Conventional MRI could also be combined with perfusion-weighted MRI. In the study by Nakagawa *et al* (56), compared with the results of two radiologists, a model that extracted features from T2WI, CE-T1WI, an ADC map and an rCBV map provided a better performance for diagnosing 25 PCNSLs and 45 GBMs.

Deep learning-based radiomics. Deep learning-based radiomics also perform well in the differential diagnosis. McAvoy *et al* (57) identified the high accuracy of convolutional neural networks (CNNs) based on CE-T1WI for the differential diagnosis between 24 CNS-DLBCLs and 35 GBMs. In a larger population (92 PCNSLs and 97 GBMs), deep learning radiomics with data enhancement performed better than two neuroradiologists (58). Another group also reported CE-T1W1-based multiparametric CNNs and showed that it had a similar accuracy to radiologists (accuracy, 0.899; P=0.886) for differentiating between 136 PCNSLs and 153 GBMs (59). For differentiating 14 atypical GBMs from 11 PCNSLs, the CE-T1WI-based deep learning model also performed well (60).

A systematic review (44) announced the suboptimal quality of radiomics studies in lymphoma and suggested further research before extensive clinical use. Most radiomics studies are retrospective without large cohorts. Additionally, there are no standard methods for image acquisition, model generation and evaluation. For example, a cohort study with small sample sizes displayed a lower AUC of CNNs (0.486) based on CE-T1WI and ADC maps compared with that of feature-based radiomics (0.947) or radiologists (0.913-0.932) to distinguish 14 PCNSLs from 28 GBMs (61). However, compared with feature-based radiomics, deep learning-based radiomics requires less time in manual feature extraction or tumor segmentation. Another radiomics model, in which the perfusion information was captured by deep learning-based radiomics, showed a similar performance to rCBV in differentiating 15 PCNSLs from 28 GBMs (62). Metabolism assessed by FDG-PET-based radiomics also showed potential value in differentiating between 24 CNS DLBCLs and 53 GBMs, with an AUC of 0.971-0.998 (41).

In summary, radiomics remains a potential tool for the discrimination between PCNSL and HGG. Details of all radiomics models and case numbers of PCNSL and GBM involved in a series of studies are summarized in Table SII.

4. Progress of CSF and blood analysis in PCNSL and HGG

Cytology and flow cytometry. CSF sampling is an additional choice other than biopsy if it is safe and does not delay the diagnostic process or treatment (7). CSF analysis includes flow cytometry and cytology, and may consider gene rearrangements (16). In cytology, GBM cells have hyperchromatic nuclei and a variable amount of cytoplasm, appearing singly or arranged in small cohesive groups, while PCNSL usually consists of a monotonous population of dyshesive large lymphoid cells (63). One study mentioned that flow cytometry of CSF improves the sensitivity up to 2-3 times more than cytology analysis (64). Furthermore, another research group (65) defined the sensitivity of cytology and flow cytometry as 13.3 and 23.3%, respectively, by analyzing the CSF of 30 patients with PCNSL. However, studies confirmed considerable diagnostic delays of PCNSL that may take up to several weeks due to lengthy cytology or flow cytometry analysis of CSF, especially under conditions of limited or rare tumor cells in CSF specimens where more procedures will be required, and detection time will be further increased (13,66). The detection of biomarkers in CSF and blood may improve the diagnosis. Diagnostic biomarkers include proteins, RNA, DNA and extracellular vesicles (EVs).

Protein. Proteins in CSF can be analyzed by latex agglutination turbidimetric immunoassay (LATIA), enzyme-linked immunosorbent assay (ELISA) and targeted proteomics assays such as selected reaction monitoring (SRM). Some proteins, such as C-X-C motif chemokine ligand 13 (CXCL13), interleukin-10 (IL-10), β2-microglobulin (B2M), soluble IL-2 receptor (sIL-2R), apolipoprotein C-II (APOC2), glycoprotein non-metastatic melanoma protein B (GPNMB), and V-set and immunoglobulin domain-containing protein 4 (VSIG4), are considered promising protein biomarkers for PCNSL in the CSF (67). CXCL13 and IL-10 are mediators of the migration and growth of B cells, respectively. B2M is a component of the major histocompatibility complex class I molecules. sIL-2R is a receptor that is mostly released by regulatory T

cells (68). APOC2 is an exchangeable apolipoprotein that activates lipoprotein lipase (69). GPNMB is an endogenous type 1 transmembrane glycoprotein (70). VSIG4 is a phagocytic receptor that negatively regulates T-cell proliferation and IL-2 production (71). All these proteins may be upregulated in the CSF of patients with PCNSL compared with patients with GBM (71-75). The combination of different biomarkers can improve diagnostic performance. Maeyama *et al* (72) proposed a multi-marker prediction algorithm that was effective (AUC, 0.994) in distinguishing 32 PCNSLs from 21 GBMs and 51 other brain lesions by incorporating the detection of CXCL13, IL-10, B2M and sIL-2R in the CSF. In the study, only B2M was measured by LATIA, while the remaining biomarkers were analyzed by ELISA. Combined analysis of APOC2, GPNMB and VSIG4 proteins in CSF was effective (AUC, 0.953) in distinguishing 28 PCNSLs from 7 GBMs 3 astrocytomas using the SRM method (71).

DNA. Alterations in tumor-specific genes and methylation of circulating tumor DNA (ctDNA) can be detected by gene-targeted PCR for the purpose of differential diagnosis, with high sensitivity (76). Cell-free DNA (cfDNA) is DNA shed from the cell into the body fluids. A portion of cfDNA is derived from tumor cells, which is referred to as ctDNA (71). The CSF sampling serves as a better choice for the detection of mutations compared with plasma, which contains less cfDNA or ctDNA than CSF due to the BBB (76-78). Myeloid differentiation primary response gene 88 (MYD88) encodes a cytosolic adapter protein that plays a central role in innate and adaptive immunity. CD79B encodes the B-cell antigen receptor complex-associated protein β chain. The alterations of L265 in MYD88 and Y196 in CD79B are detected in recurrent lymphoid tumors. A large cohort study (79) detected mutations in MYD88 L265 and CD79B Y196 in 71.7% and 64.2% of CNS DLBCL cases, respectively, but no MYD88 or CD79B mutations were detected in GBM. Hiemcke-Jiwa *et al* (80) used the droplet digital PCR method to detect MYD88 mutation in cfDNA and found that 8 out of 11 CSF specimens from PCNSL were positive, including 2 unknown PCNSL samples and 6 CNS DLBCL samples, while all CSF samples from 3 GBMs were negative for the mutation. Combining gene mutations with protein markers can improve diagnostic performance. Ferreri *et al* (81) combined MYD88 mutational status (assessed by TaqMan-based PCR) with IL-10 levels in CSF and differentiated 36 PCNSLs from 106 other CNS diseases (10 GBMs), with 94% sensitivity and 98% specificity. Furthermore, certain methylated DNA markers can provide valuable diagnostic clues for differentiation. Wang *et al* (77) detected the methylation of MGMT promoter in ctDNA in 18 out of 28 CSF samples from HGG using methylation-specific PCR. Recently, Downs *et al* (82) identified methylation markers cg054 and SCG3 in plasma via a novel method of tailed amplicon multiplexed-methylation-specific PCR, with a high level of accuracy to distinguish PCNSLs from other CNS tumors.

RNA. Different physiological and pathological processes between PCNSL and GBM can also be reflected by extracellular RNAs (exRNAs), such as small non-coding RNA (ncRNA) (83), which freely exist in body fluids or concentrated

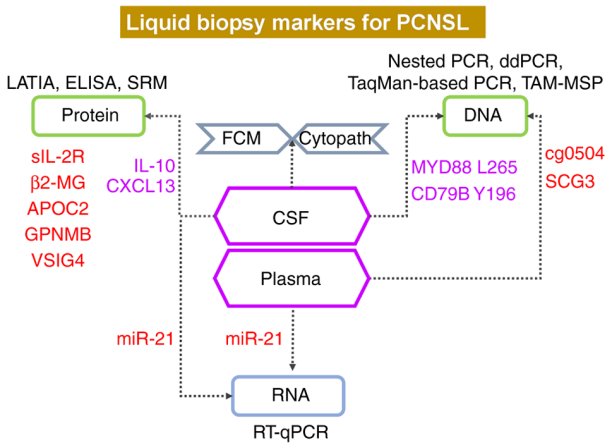

Figure 3. Prospects in liquid biopsy biomarkers of the CSF and plasma. Among these markers, CXCL13 and IL-10 in the CSF show more supportive evidence. Since diffuse large B-cell lymphoma accounts for most PCNSL cases, MYD88 L265 and CD79B Y196 in the CSF are meaningful for the diagnosis of PCNSL. Other promising evidence, such as increased miR-21 level in the CSF and plasma, increased cg0504 and SCG3 levels in the plasma, and increased sIL-2R, β2-MG, APOC2, GPNMB and VSIG4 levels in the CSF, also suggest PCNSL. CSF, cerebrospinal fluid; CXCL13, C-X-C motif chemokine ligand 13; IL-10, interleukin-10; B2M, β2-microglobulin; sIL-2R, soluble IL-2 receptor; APOC2, apolipoprotein C-II; GPNMB, glycoprotein non-metastatic melanoma protein B; VSIG4, V-set and immunoglobulin domain-containing protein 4; PCNSL, primary central nervous system lymphoma; miR, microRNA; LATIA, latex agglutination turbidimetric immunoassay; ELISA, enzyme-linked immunosorbent assay; SRM, selected reaction monitoring; FCM, flow cytometry; cytopath, cytopathology; RT-qPCR, reverse-transcription-quantitative PCR; ddPCR, droplet digital PCR; TAM-MSP, tailed amplicon multiplexed-methylation-specific PCR; MYD88, myeloid differentiation primary response gene 88.

in carriers such as EVs (84). MicroRNAs (miRNAs/miRs) are snRNAs of 18 to 24 nucleotides in length (85). EVs are small lipid bilayer-enclosed vesicles containing proteins, lipids and nucleic acids that release from cells (86). A number of exRNAs, such as free miRNA (miR-15b and miR-21) and RNA in EVs (RNU6-1) have been used to differentiate between PCNSL and GBM in previous studies (87). miR-15b is important in glioma carcinogenesis for regulating cell cycle progression (88). One study reported higher miR-15b levels in the CSF of 10 gliomas compared with those in 23 PCNSLs and 17 other CNS diseases, with an AUC of 0.960 (89). miR-21 is one of the most highly expressed miRNAs and mainly targets the phosphatase and tensin homologue (PTEN) gene (90). A previous study showed that PCNSL cases displayed relatively higher miR-21 levels compared with those in patients with GBM and healthy individuals. miR-21 levels are higher in the CSF (89) and serum (87) of B-cell type PCNSL than those of GBM. RNU6-1 is an snRNA that is negatively regulated by the PTEN pathway (91). More alterations of the PTEN pathway in GBM than in PCNSL leads to higher RNU6-1 expression (92). A study showed that high levels of RNU6-1 in EVs derived from serum helped differentiate between 18 GBMs and 12 PCNSLs, with an AUC of 0.700 (92). Overall, the limited studies on miRNAs with regard to distinguishing PCNSL from HGG have presented heterogeneous results without consistent expression variation across cohorts due to the lack of standards for liquid collection, RNA extraction, RNA sequencing and statistical analysis. A large cohort with

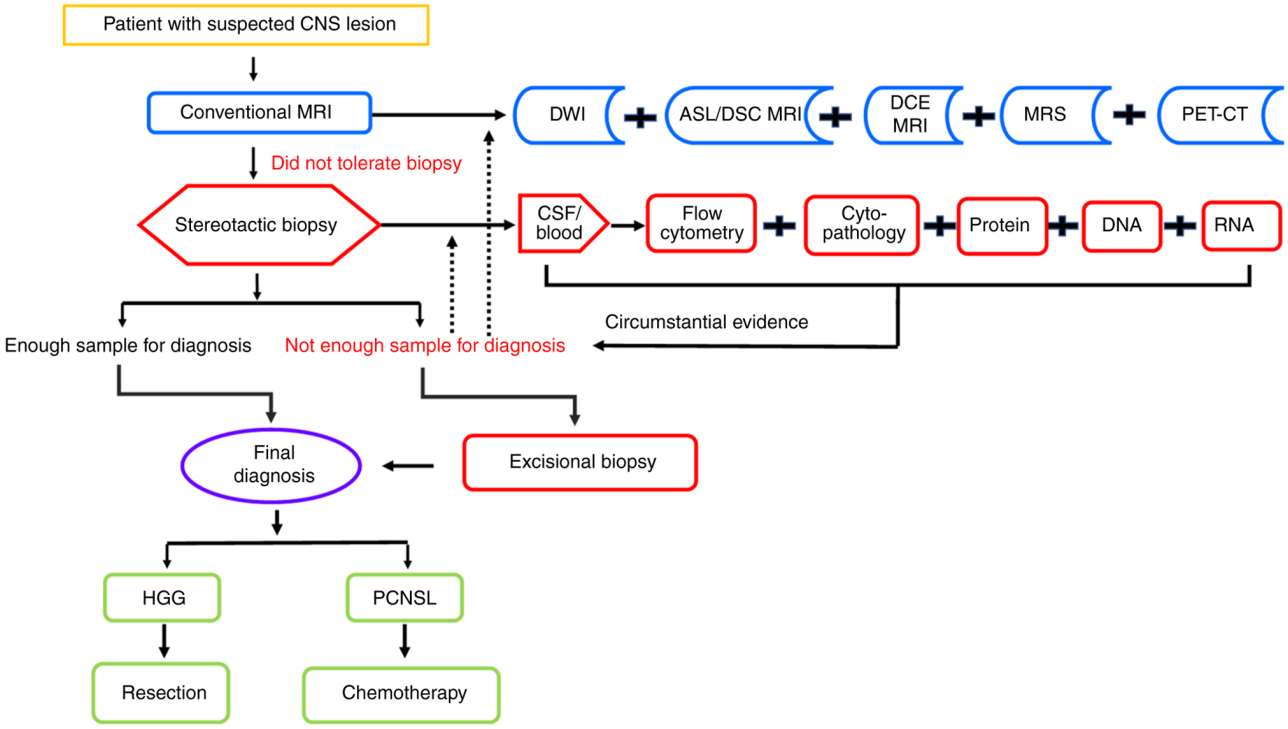

Figure 4. Integrated radiological-pathological evidence for the differential diagnosis of PCNSL from HGG. For patients with suspected CNS lesions, conventional MRI is preferred before stereotactic biopsy. If a biopsy is not tolerated or the specimen is limited, a selective combination of advanced MRI (including DWI, ASL/DSC MRI and DCE MRI), PET-CT and liquid biopsy will provide circumstantial evidence for the differential diagnosis. CNS, central nervous system; MRI, magnetic resonance imaging; DWI, diffusion-weighted imaging; ASL, arterial spin labeling; DSC, dynamic susceptibility contrast; DCE, dynamic contrast-enhanced; MRI, magnetic resonance imaging; MRS, magnetic resonance spectroscopy; PET/CT, positron emission tomography/computed tomography; CSF, cerebrospinal fluid; PCNSL, primary central nervous system lymphoma; HGG, high-grade glioma.

comparative research of the aforementioned miRNAs will be meaningful for potential clinical application.

Preferred liquid biomarkers for the differential diagnosis of PCNSL from HGG. Details of all of the liquid parameters and case numbers of PCNSL and GBM involved in a series of studies are summarized in Table SIII. Among these data, as shown in Fig. 3, examinations of CXCL13 and IL-10 showed more supportive evidence. Since DLBCL accounts for most PCNSL cases, MYD88 L265 and CD79B Y196 in the CSF are meaningful for the diagnosis of PCNSL. Other promising evidence, such as an increased miR-21 level in the CSF and plasma, increased cg0504 and SCG3 levels in the plasma, and increased sIL-2R, β2-MG, APOC2, GPNMB and VSIG4 levels in the CSF, are also suggestive of PCNSL, yet further evidence is required.

5. Promising combination studies of multiple analyses

Combining different detection methods or parameters may provide more accurate and robust support for diagnosis (Table SIV). Combined technologies, including MRI and DWI, have most commonly been used (22,23,93). A previous study (22) combined rADC with K^{trans} to distinguish 18 CNS DLBCLs from 42 GBMs, and this method performed better than using each parameter alone. Makino *et al* (23) designed a two-step decision tree with an $rCBV_{max}$ of 4 and ADC_{min} of 1. The combination facilitated differentiation between 33 PCNSLs and 54 GBMs. Another study (93) showed that the combination of mean and maximum CBV, mean and maximum selective ADC, and $rCBV_{mean}$ could obtain 100% accuracy for discrimination between 37 PCNSLs and 37 GBMs. A corporation analysis of diffusion and susceptibility also showed a good performance (18). Ozturk *et al* (18) combined rSWI with $rADC_{mean}$ to differentiate 31 B-cell type PCNSLs with BCL2 and MYC rearrangements from 57 atypical GBMs without visible necrosis. The combination improved the diagnostic performance to an AUC of 0.936. Saini *et al* (37) used ADC, corrected rCBV, back flux exchange rate and ITSS scores to perform a multiparametric assessment of 30 B-cell PCNSLs and 70 GBMs. The study reported the good performance of this model, with an AUC of 0.920. A combination of ADC values and biomarker analysis has also been used in research (94), including the average ADC, and CXCL13 and IL-10 levels in the CSF, with a better performance than any single variable model. Recently, a combination of 18F-FDG-PET and ASL was also introduced to differentiate PCNSL from GBM, which achieved a better performance than either technique alone (95). Yet, to the best of our knowledge, there is no standard multiparametric model that has been assessed prospectively in a large population. Further studies are needed.

6. Conclusions and future prospects

Accurate diagnosis is a prerequisite for the precise treatment of PCNSL and GBM. Multidisciplinary participation, including clinicians, radiologists and pathologists, is meaningful for improving the accuracy and speed of the decision-making

process. However, most of the radiological and pathological markers discussed within the present review are from retrospective small-scale and heterogeneous cohorts. Thus, current evidence from these studies shows the limited quality of radiological and liquid biopsy, which is unable to replace the need for histology examination.

Although stereotactic biopsy is an optimal choice for diagnosis, it is not always conclusive. Otherwise, surgical resection may be another option, not only for providing enough pathological specimens but also for significantly improving the overall survival and progression-free survival of certain patients with PCNSL (96,97). A recent systematic review highlighted the possible benefit of cytoreductive surgery in PCNSL (98). Another recent study reported that resection significantly prolonged the survival of patients <70 years old with superficial solitary lymphoma lesions (99). However, when lymphoma lesions are deeply seated, it is frequently not amenable to resect them, and biopsy will be a safer option (99,100).

Although radiological examination, and CSF and blood analysis are useful for the diagnosis of PCNSL, it is not always practical in clinical due to the economic and staff/equipment time aspects. Thus, as shown in Fig. 4, based on the literature, we propose an optional procedure using multiparametric imaging technologies and liquid biopsies to improve the diagnostic performance and management of CNS neoplasms, especially PCNSL. More evidence should be collected in the future for the clinical management of PCNSL and in order to make the current diagnostic workflow more reasonable and practical.

Acknowledgements

Not applicable.

Funding

This study was supported by the Young Scientists Fund of the National Natural Science Foundation of China (grant no. 81700198), the Science and Technology Development Project of Jilin Province (grant no. 20190701064GH), the Open Project of Key Laboratory of Tumor Immunology and Pathology (Army Medical University), Ministry of Education (grant no. 2018jsz101) and the College Student Innovation and Entrepreneurship Training Program of Jilin University (grant no. 202010183X453).

Availability of data and materials

Not applicable.

Authors' contributions

XJW developed the concept, designed the study and revised the manuscript. LMC collected the literature and wrote the draft. MCZ and YZ respectively reorganized the context in radiology and liquid biopsy. LMC, MCZ and YZ contributed equally. BJ and XMW respectively contributed suggestions on PET-CT and pathology. MCZ, YZ, BJ and LMC participated in writing or revising the review. All authors read and approved the final manuscript. Data authentication is not applicable.

Ethics approval and consent to participate

Not applicable.

Patient consent for publication

Written informed consent was obtained from the individuals for the publication of any potentially identifiable images or data included in this article.

Competing interests

The authors declare that they have no competing interests.

References

1. Ostrom QT, Price M, Neff C, Cioffi G, Waite KA, Kruchko C and Barnholtz-Sloan JS: CBTRUS statistical report: Primary brain and other central nervous system tumors diagnosed in the United States in 2015-2019. Neuro Oncol 24 (Suppl 5): v1-v95, 2022.
2. Fox CP, Phillips EH, Smith J, Linton K, Gallop-Evans E, Hemmaway C, Auer DP, Fuller C, Davies AJ, McKay P, *et al*: Guidelines for the diagnosis and management of primary central nervous system diffuse large B-cell lymphoma. Br J Haematol 184: 348-363, 2019.
3. Sugita Y, Muta H, Ohshima K, Morioka M, Tsukamoto Y, Takahashi H and Kakita A: Primary central nervous system lymphomas and related diseases: Pathological characteristics and discussion of the differential diagnosis. Neuropathology 36: 313-324, 2016.
4. Grommes C, Rubenstein JL, DeAngelis LM, Ferreri AJM and Batchelor TT: Comprehensive approach to diagnosis and treatment of newly diagnosed primary CNS lymphoma. Neuro Oncol 21: 296-305, 2019.
5. McKinnon C, Nandhabalan M, Murray SA and Plaha P: Glioblastoma: Clinical presentation, diagnosis, and management. BMJ 374: n1560, 2021.
6. Alexander BM and Cloughesy TF: Adult Glioblastoma. J Clin Oncol 35: 2402-2409, 2017.
7. Chiavazza C, Pellerino A, Ferrio F, Cistaro A, Soffietti R and Ruda R: Primary CNS lymphomas: Challenges in diagnosis and monitoring. Biomed Res Int 2018: 3606970, 2018.
8. Grommes C and DeAngelis LM: Primary CNS Lymphoma. J Clin Oncol 35: 2410-2418, 2017.
9. Su L, Ding M, Chen L, Li C and Lao M: Primary central nervous system lymphoma in a patient with systemic lupus erythematosus mimicking high-grade glioma: A case report and review of literature. Medicine (Baltimore) 97: e11072, 2018.
10. Bhatt VR, Shrestha R, Shonka N and Bociek RG: Near misdiagnosis of glioblastoma as primary central nervous system lymphoma. J Clin Med Res 6: 299-301, 2014.
11. Louis DN, Perry A, Reifenberger G, von Deimling A, Figarella-Branger D, Cavenee WK, Ohgaki H, Wiestler OD, Kleihues P and Ellison DW: The 2016 World Health organization classification of tumors of the central nervous system: A summary. Acta Neuropathol 131: 803-820, 2016.
12. Giannini C, Dogan A and Salomão DR: CNS Lymphoma: A practical diagnostic approach. J Neuropathol Exp Neurol 73: 478-494, 2014.
13. Morell AA, Shah AH, Cavallo C, Eichberg DG, Sarkiss CA, Benveniste R, Ivan ME and Komotar RJ: Diagnosis of primary central nervous system lymphoma: A systematic review of the utility of CSF screening and the role of early brain biopsy. Neurooncol Pract 6: 415-423, 2019.
14. Patrick LB and Mohile NA: Advances in primary central nervous system lymphoma. Curr Oncol Rep 17: 60, 2015.
15. Velasco R, Mercadal S, Vidal N, Alañá M, Barceló MI, Ibáñez-Juliá MJ, Bobillo S, Caldú Agud R, García Molina E, Martínez P, *et al*: Diagnostic delay and outcome in immunocompetent patients with primary central nervous system lymphoma in Spain: A multicentric study. J Neurooncol 148: 545-554, 2020.

16. Nabors LB, Portnow J, Baehring J, Bloch O, Brem S, Butowski N, Cannon DM, Chao S, Chheda MG, Clark SW, *et al*: NCCN Clinical Practice Guidelines in Oncology Central Nervous System Cancers (Version 2.2022 - September 29, 2022). https://www.nccn.org/guidelines/guidelines-detail?category=1&id=1425
17. Chukwueke UN and Nayak L: Central nervous system lymphoma. Hematol Oncol Clin North Am 33: 597-611, 2019.
18. Ozturk K, Soylu E and Cayci Z: Differentiation between primary CNS lymphoma and atypical glioblastoma according to major genomic alterations using diffusion and susceptibility-weighted MR imaging. Eur J Radiol 141: 109784, 2021.
19. Barajas RF, Politi LS, Anzalone N, Schöder H, Fox CP, Boxerman JL, Kaufmann TJ, Quarles CC, Ellingson BM, Auer D, *et al*: Consensus recommendations for MRI and PET imaging of primary central nervous system lymphoma: Guideline statement from the International primary CNS lymphoma collaborative group (IPCG). Neuro Oncol 23: 1056-1071, 2021.
20. Villanueva-Meyer JE, Mabray MC and Cha S: Current clinical brain tumor imaging. Neurosurgery 81: 397-415, 2017.
21. Lin X, Lee M, Buck O, Woo KM, Zhang Z, Hatzoglou V, Omuro A, Arevalo-Perez J, Thomas AA, Huse J, *et al*: Diagnostic accuracy of T1-Weighted dynamic contrast-enhanced-MRI and DWI-ADC for differentiation of glioblastoma and primary CNS Lymphoma. AJNR Am J Neuroradiol 38: 485-491, 2017.
22. Lu S, Wang S, Gao Q, Zhou M, Li Y, Cao P, Hong X and Shi H: Quantitative evaluation of diffusion and dynamic contrast-enhanced magnetic resonance imaging for differentiation between primary central nervous system lymphoma and glioblastoma. J Comput Assist Tomogr 41: 898-903, 2017.
23. Makino K, Hirai T, Nakamura H, Kuroda JI, Shinojima N, Uetani H, Kitajima M and Yano S: Differentiating between primary central nervous system lymphomas and glioblastomas: Combined use of perfusion-weighted and diffusion-weighted magnetic resonance imaging. World Neurosurg 112: e1-e6, 2018.
24. Ahn SJ, Shin HJ, Chang JH and Lee SK: Differentiation between primary cerebral lymphoma and glioblastoma using the apparent diffusion coefficient: Comparison of three different ROI methods. PLoS One 9: e112948, 2014.
25. Nakajima S, Okada T, Yamamoto A, Kanagaki M, Fushimi Y, Okada T, Arakawa Y, Takagi Y, Miyamoto S and Togashi K: Primary central nervous system lymphoma and glioblastoma: Differentiation using dynamic susceptibility-contrast perfusion-weighted imaging, diffusion-weighted imaging, and (18)F-fluorodeoxyglucose positron emission tomography. Clin Imaging 39: 390-395, 2015.
26. Suh CH, Kim HS, Jung SC, Choi CG and Kim SJ: Clinically relevant imaging features for MGMT promoter methylation in multiple glioblastoma studies: A systematic review and meta-analysis. AJNR Am J Neuroradiol 39: 1439-1445, 2018.
27. Akbari H, Bakas S, Pisapia JM, Nasrallah MP, Rozycki M, Martinez-Lage M, Morrissette JJD, Dahmane N, O'Rourke DM and Davatzikos C: In vivo evaluation of EGFRvIII mutation in primary glioblastoma patients via complex multiparametric MRI signature. Neuro Oncol 20: 1068-1079, 2018.
28. Quarles CC, Bell LC and Stokes AM: Imaging vascular and hemodynamic features of the brain using dynamic susceptibility contrast and dynamic contrast enhanced MRI. Neuroimage 187: 32-55, 2019.
29. Suh CH, Kim HS, Jung SC, Park JE, Choi CG and Kim SJ: MRI as a diagnostic biomarker for differentiating primary central nervous system lymphoma from glioblastoma: A systematic review and meta-analysis. J Magn Reson Imaging 50: 560-572, 2019.
30. Neska-Matuszewska M, Bladowska J, Sasiadek M and Zimny A: Differentiation of glioblastoma multiforme, metastases and primary central nervous system lymphomas using multiparametric perfusion and diffusion MR imaging of a tumor core and a peritumoral zone-Searching for a practical approach. PLoS One 13: e0191341, 2018.
31. Xu W, Wang Q, Shao A, Xu B and Zhang J: The performance of MR perfusion-weighted imaging for the differentiation of high-grade glioma from primary central nervous system lymphoma: A systematic review and meta-analysis. PLoS One 12: e0173430, 2017.
32. Cindil E, Sendur HN, Cerit MN, Dag N, Erdogan N, Celebi FE, Oner Y and Tali T: Validation of combined use of DWI and percentage signal recovery-optimized protocol of DSC-MRI in differentiation of high-grade glioma, metastasis, and lymphoma. Neuroradiology 63: 331-342, 2021.
33. Chaganti J, Taylor M, Woodford H and Steel T: Differentiation of primary central nervous system lymphoma and high-grade glioma with dynamic susceptibility contrast-derived metrics: Pilot study. World Neurosurg 151: e979-e987, 2021.
34. Semmineh NB, Xu J, Skinner JT, Xie J, Li H, Ayers G and Quarles CC: Assessing tumor cytoarchitecture using multiecho DSC-MRI derived measures of the transverse relaxivity at tracer equilibrium (TRATE). Magn Reson Med 74: 772-784, 2015.
35. Lee MD, Baird GL, Bell LC, Quarles CC and Boxerman JL: Utility of percentage signal recovery and baseline signal in DSC-MRI optimized for relative CBV measurement for differentiating glioblastoma, lymphoma, metastasis, and meningioma. AJNR Am J Neuroradiol 40: 1445-1450, 2019.
36. Hsu CC, Watkins TW, Kwan GN and Haacke EM: Susceptibility-Weighted imaging of glioma: Update on current imaging status and future directions. J Neuroimaging 26: 383-390, 2016.
37. Saini J, Kumar Gupta P, Awasthi A, Pandey CM, Singh A, Patir R, Ahlawat S, Sadashiva N, Mahadevan A and Kumar Gupta R: Multiparametric imaging-based differentiation of lymphoma and glioblastoma: Using T1-perfusion, diffusion, and susceptibility-weighted MRI. Clin Radiol 73: 986 e7-986 e15, 2018.
38. Yamasaki F, Takayasu T, Nosaka R, Amatya VJ, Doskaliyev A, Akiyama Y, Tominaga A, Takeshima Y, Sugiyama K and Kurisu K: Magnetic resonance spectroscopy detection of high lipid levels in intraaxial tumors without central necrosis: A characteristic of malignant lymphoma. J Neurosurg 122: 1370-1379, 2015.
39. Nagashima H, Sasayama T, Tanaka K, Kyotani K, Sato N, Maeyama M, Kohta M, Sakata J, Yamamoto Y, Hosoda K, *et al*: Myo-inositol concentration in MR spectroscopy for differentiating high grade glioma from primary central nervous system lymphoma. J Neurooncol 136: 317-326, 2018.
40. Nomura Y, Asano Y, Shinoda J, Yano H, Ikegame Y, Kawasaki T, Nakayama N, Maruyama T, Muragaki Y and Iwama T: Characteristics of time-activity curves obtained from dynamic ^{11}C-methionine PET in common primary brain tumors. J Neurooncol 138: 649-658, 2018.
41. Kong Z, Jiang C, Zhu R, Feng S, Wang Y, Li J, Chen W, Liu P, Zhao D, Ma W, *et al*: ^{18}F-FDG-PET-based radiomics features to distinguish primary central nervous system lymphoma from glioblastoma. Neuroimage Clin 23: 101912, 2019.
42. Zhou W, Wen J, Hua F, Xu W, Lu X, Yin B, Geng D and Guan Y: ^{18}F-FDG PET/CT in immunocompetent patients with primary central nervous system lymphoma: Differentiation from glioblastoma and correlation with DWI. Eur J Radiol 104: 26-32, 2018.
43. Kim HO, Kim JS, Kim SO, Chae SY, Oh SJ, Seo M, Lee SH, Oh JS, Ryu JS, Huh JR and Kim JH: Clinicopathological characteristics of primary central nervous system lymphoma with low 18F-fludeoxyglucose uptake on brain positron emission tomography. Medicine (Baltimore) 99: e20140, 2020.
44. Wang H, Zhou Y, Li L, Hou W, Ma X and Tian R: Current status and quality of radiomics studies in lymphoma: A systematic review. Eur Radiol 30: 6228-6240, 2020.
45. Lohmann P, Galldiks N, Kocher M, Heinzel A, Filss CP, Stegmayr C, Mottaghy FM, Fink GR, Jon Shah N and Langen KJ: Radiomics in neuro-oncology: Basics, workflow, and applications. Methods 188: 112-121, 2021.
46. Priya S, Ward C, Locke T, Soni N, Maheshwarappa RP, Monga V, Agarwal A and Bathla G: Glioblastoma and primary central nervous system lymphoma: Differentiation using MRI derived first-order texture analysis-a machine learning study. Neuroradiol J 34: 320-328, 2021.
47. Han Y, Wang ZJ, Li WH, Yang Y, Zhang J, Yang XB, Zuo L, Xiao G, Wang SZ, Yan LF and Cui GB: Differentiation between primary central nervous system lymphoma and atypical glioblastoma based on MRI morphological feature and signal intensity ratio: A retrospective multicenter study. Front Oncol 12: 811197, 2022.
48. Suh HB, Choi YS, Bae S, Ahn SS, Chang JH, Kang SG, Kim EH, Kim SH and Lee SK: Primary central nervous system lymphoma and atypical glioblastoma: Differentiation using radiomics approach. Eur Radiol 28: 3832-3839, 2018.
49. Chen C, Zheng A, Ou X, Wang J and Ma X: Comparison of radiomics-based machine-learning classifiers in diagnosis of glioblastoma from primary central nervous system lymphoma. Front Oncol 10: 1151, 2020.

50. MacIver CL, Busaidi AA, Ganeshan B, Maynard JA, Wastling S, Hyare H, Brandner S, Markus JE, Lewis MA, Groves AM, *et al*: Filtration-Histogram based magnetic resonance texture analysis (MRTA) for the distinction of primary central nervous system lymphoma and glioblastoma. J Pers Med 11: 876, 2021.
51. Mehrnahad M, Rostami S, Kimia F, Kord R, Taheri MS, Rad HS, Haghighatkhah H, Moradi A and Kord A: Differentiating glioblastoma multiforme from cerebral lymphoma: Application of advanced texture analysis of quantitative apparent diffusion coefficients. Neuroradiol J 33: 428-436, 2020.
52. Kang D, Park JE, Kim YH, Kim JH, Oh JY, Kim J, Kim Y, Kim ST and Kim HS: Diffusion radiomics as a diagnostic model for atypical manifestation of primary central nervous system lymphoma: Development and multicenter external validation. Neuro Oncol 20: 1251-1261, 2018.
53. Xia W, Hu B, Li H, Geng C, Wu Q, Yang L, Yin B, Gao X, Li Y and Geng D: Multiparametric-MRI-Based radiomics model for differentiating primary central nervous system lymphoma from glioblastoma: Development and cross-vendor validation. J Magn Reson Imaging 53: 242-250, 2021.
54. Kim Y, Cho HH, Kim ST, Park H, Nam D and Kong DS: Radiomics features to distinguish glioblastoma from primary central nervous system lymphoma on multi-parametric MRI. Neuroradiology 60: 1297-1305, 2018.
55. Bathla G, Priya S, Liu Y, Ward C, Le NH, Soni N, Maheshwarappa RP, Monga V, Zhang H and Sonka M: Radiomics-based differentiation between glioblastoma and primary central nervous system lymphoma: A comparison of diagnostic performance across different MRI sequences and machine learning techniques. Eur Radiol 31: 8703-8713, 2021.
56. Nakagawa M, Nakaura T, Namimoto T, Kitajima M, Uetani H, Tateishi M, Oda S, Utsunomiya D, Makino K, Nakamura H, *et al*: Machine learning based on multi-parametric magnetic resonance imaging to differentiate glioblastoma multiforme from primary cerebral nervous system lymphoma. Eur J Radiol 108: 147-154, 2018.
57. McAvoy M, Prieto PC, Kaczmarzyk JR, Fernández IS, McNulty J, Smith T, Yu KH, Gormley WB and Arnaout O: Classification of glioblastoma versus primary central nervous system lymphoma using convolutional neural networks. Sci Rep 11: 15219, 2021.
58. Zhang Y, Liang K, He J, Ma H, Chen H, Zheng F, Zhang L, Wang X, Ma X and Chen X: Deep learning with data enhancement for the differentiation of solitary and multiple cerebral glioblastoma, lymphoma, and tumefactive demyelinating lesion. Front Oncol 11: 665891, 2021.
59. Xia W, Hu B, Li H, Shi W, Tang Y, Yu Y, Geng C, Wu Q, Yang L, Yu Z, *et al*: Deep learning for automatic differential diagnosis of primary central nervous system lymphoma and glioblastoma: Multi-Parametric magnetic resonance imaging based convolutional neural network model. J Magn Reson Imaging 54: 880-887, 2021.
60. Tariciotti L, Caccavella VM, Fiore G, Schisano L, Carrabba G, Borsa S, Giordano M, Palmisciano P, Remoli G, Remore LG, *et al*: A deep learning model for preoperative differentiation of glioblastoma, brain metastasis and primary central nervous system lymphoma: A pilot study. Front Oncol 12: 816638, 2022.
61. Yun J, Park JE, Lee H, Ham S, Kim N and Kim HS: Radiomic features and multilayer perceptron network classifier: A robust MRI classification strategy for distinguishing glioblastoma from primary central nervous system lymphoma. Sci Rep 9: 5746, 2019.
62. Park JE, Kim HS, Lee J, Cheong EN, Shin I, Ahn SS and Shim WH: Deep-learned time-signal intensity pattern analysis using an autoencoder captures magnetic resonance perfusion heterogeneity for brain tumor differentiation. Sci Rep 10: 21485, 2020.
63. Chhieng DC, Elgert P, Cohen JM, Jhala NC and Cangiarella JF: Cytology of primary central nervous system neoplasms in cerebrospinal fluid specimens. Diagn Cytopathol 26: 209-212, 2002.
64. Bromberg JE, Breems DA, Kraan J, Bikker G, van der Holt B, Smitt PS, van den Bent MJ, van't Veer M and Gratama JW: CSF flow cytometry greatly improves diagnostic accuracy in CNS hematologic malignancies. Neurology 68: 1674-1679, 2007.
65. Schroers R, Baraniskin A, Heute C, Vorgerd M, Brunn A, Kuhnhenn J, Kowoll A, Alekseyev A, Schmiegel W, Schlegel U, *et al*: Diagnosis of leptomeningeal disease in diffuse large B-cell lymphomas of the central nervous system by flow cytometry and cytopathology. Eur J Haematol 85: 520-528, 2020.
66. Baraniskin A, Deckert M, Schulte-Altedorneburg G, Schlegel U and Schroers R: Current strategies in the diagnosis of diffuse large B-cell lymphoma of the central nervous system. Br J Haematol 156: 421-432, 2012.
67. van Westrhenen A, Smidt LCA, Seute T, Nierkens S, Stork ACJ, Minnema MC and Snijders TJ: Diagnostic markers for CNS lymphoma in blood and cerebrospinal fluid: A systematic review. Br J Haematol 182: 384-403, 2018.
68. Yang ZZ, Grote DM, Ziesmer SC, Manske MK, Witzig TE, Novak AJ and Ansell SM: Soluble IL-2Rα facilitates IL-2-mediated immune responses and predicts reduced survival in follicular B-cell non-Hodgkin lymphoma. Blood 118: 2809-2820, 2011.
69. Wolska A, Reimund M and Remaley AT: Apolipoprotein C-II: The re-emergence of a forgotten factor. Curr Opin Lipidol 31: 147-153, 2020.
70. Saade M, Araujo de Souza G, Scavone C and Kinoshita PF: The Role of GPNMB in inflammation. Front Immunol 12: 674739, 2021.
71. Waldera-Lupa DM, Poschmann G, Kirchgaessler N, Etemad-Parishanzadeh O, Baberg F, Brocksieper M, Seidel S, Kowalski T, Brunn A, Haghikia A, *et al*: A multiplex assay for the stratification of patients with primary central nervous system lymphoma using targeted mass spectrometry. Cancers (Basel) 12: 1732, 2020.
72. Maeyama M, Sasayama T, Tanaka K, Nakamizo S, Tanaka H, Nishihara M, Fujita Y, Sekiguchi K, Kohta M, Mizukawa K, *et al*: Multi-marker algorithms based on CXCL13, IL-10, sIL-2 receptor, and β2-microglobulin in cerebrospinal fluid to diagnose CNS lymphoma. Cancer Med 9: 4114-4125, 2020.
73. Rubenstein JL, Wong VS, Kadoch C, Gao HX, Barajas R, Chen L, Josephson SA, Scott B, Douglas V, Maiti M, *et al*: CXCL13 plus interleukin 10 is highly specific for the diagnosis of CNS lymphoma. Blood 121: 4740-4748, 2013.
74. Shao J, Chen K, Li Q, Ma J, Ma Y, Lin Z, Kang H and Chen B: High level of IL-10 in cerebrospinal fluid is specific for diagnosis of primary central nervous system lymphoma. Cancer Manag Res 12: 6261-6268, 2020.
75. Masouris I, Manz K, Pfirrmann M, Dreyling M, Angele B, Straube A, Langer S, Huber M, Koedel U and Von Baumgarten L: CXCL13 and CXCL9 CSF levels in central nervous system lymphoma-diagnostic, therapeutic, and prognostic relevance. Front Neurol 12: 654543, 2021.
76. McEwen AE, Leary SES and Lockwood CM: Beyond the blood: CSF-Derived cfDNA for diagnosis and characterization of CNS tumors. Front Cell Dev Biol 8: 45, 2020.
77. Wang Z, Jiang W, Wang Y, Guo Y, Cong Z, Du F and Song B: MGMT promoter methylation in serum and cerebrospinal fluid as a tumor-specific biomarker of glioma. Biomed Rep 3: 543-548, 2015.
78. Juratli TA, Stasik S, Zolal A, Schuster C, Richter S, Daubner D, Juratli MA, Thowe R, Hennig S, Makina M, *et al*: TERT promoter mutation detection in cell-free tumor-derived DNA in patients with IDH wild-type glioblastomas: A pilot prospective study. Clin Cancer Res 24: 5282-5291, 2018.
79. Nakamura T, Tateishi K, Niwa T, Matsushita Y, Tamura K, Kinoshita M, Tanaka K, Fukushima S, Takami H, Arita H, *et al*: Recurrent mutations of CD79B and MYD88 are the hallmark of primary central nervous system lymphomas. Neuropathol Appl Neurobiol 42: 279-290, 2016.
80. Hiemcke-Jiwa LS, Leguit RJ, Snijders TJ, Bromberg JEC, Nierkens S, Jiwa NM, Minnema MC and Huibers MMH: MYD88 p.(L265P) detection on cell-free DNA in liquid biopsies of patients with primary central nervous system lymphoma. Br J Haematol 185: 974-977, 2019.
81. Ferreri AJM, Calimeri T, Lopedote P, Francaviglia I, Daverio R, Iacona C, Belloni C, Steffanoni S, Gulino A, Anghileri E, *et al*: MYD88 L265P mutation and interleukin-10 detection in cerebrospinal fluid are highly specific discriminating markers in patients with primary central nervous system lymphoma: Results from a prospective study. Br J Haematol 193: 497-505, 2021.
82. Downs BM, Ding W, Cope LM, Umbricht CB, Li W, He H, Ke X, Holdhoff M, Bettegowda C, Tao W and Sukumar S: Methylated markers accurately distinguish primary central nervous system lymphomas (PCNSL) from other CNS tumors. Clin Epigenetics 13: 104, 2021.
83. Jelski W and Mroczko B: Molecular and circulating biomarkers of brain tumors. Int J Mol Sci 22: 7039, 2021.
84. Kim S, Jeon OH and Jeon YJ: Extracellular RNA: Emerging roles in cancer cell communication and biomarkers. Cancer Lett 495: 33-40, 2020.
85. Birkó Z, Nagy B, Klekner Á and Virga J: Novel molecular markers in glioblastoma-benefits of liquid biopsy. Int J Mol Sci 21: 7522, 2020.

86. Colombo M, Raposo G and Théry C: Biogenesis, secretion, and intercellular interactions of exosomes and other extracellular vesicles. Annu Rev Cell Dev Biol 30: 255-289, 2014.
87. Yang K, Wang S, Cheng Y, Tian Y and Hou J: Role of miRNA-21 in the diagnosis and prediction of treatment efficacy of primary central nervous system lymphoma. Oncol Lett 17: 3475-3481, 2019.
88. Xia H, Qi Y, Ng SS, Chen X, Chen S, Fang M, Li D, Zhao Y, Ge R, Li G, *et al*: MicroRNA-15b regulates cell cycle progression by targeting cyclins in glioma cells. Biochem Biophys Res Commun 380: 205-210, 2009.
89. Baraniskin A, Kuhnhenn J, Schlegel U, Maghnouj A, Zollner H, Schmiegel W, Hahn S and Schroers R: Identification of microRNAs in the cerebrospinal fluid as biomarker for the diagnosis of glioma. Neuro Oncol 14: 29-33, 2012.
90. Meng F, Henson R, Wehbe-Janek H, Ghoshal K, Jacob ST and Patel T: MicroRNA-21 regulates expression of the PTEN tumor suppressor gene in human hepatocellular cancer. Gastroenterology 133: 647-658, 2007.
91. Cabarcas S, Watabe K and Schramm L: Inhibition of U6 snRNA transcription by PTEN. Online J Biol Sci 10: 114-125, 2010.
92. Puigdelloses M, Gonzalez-Huarriz M, Garcia-Moure M, Martinez-Velez N, Esparragosa Vazquez I, Bruna J, Zandio B, Agirre A, Marigil M, Petrirena G, *et al*: RNU6-1 in circulating exosomes differentiates GBM from non-neoplastic brain lesions and PCNSL but not from brain metastases. Neurooncol Adv 2: vdaa010, 2020.
93. Eisenhut F, Schmidt MA, Putz F, Lettmaier S, Fröhlich K, Arinrad S, Coras R, Luecking H, Lang S, Fietkau R and Doerfler A: Classification of primary cerebral lymphoma and glioblastoma featuring dynamic susceptibility contrast and apparent diffusion coefficient. Brain Sci 10: 886, 2020.
94. Mabray MC, Barajas RF, Villanueva-Meyer JE, Zhang CA, Valles FE, Rubenstein JL and Cha S: The combined performance of ADC, CSF CXC Chemokine Ligand 13, and CSF Interleukin 10 in the diagnosis of central nervous system lymphoma. AJNR Am J Neuroradiol 37: 74-79, 2016.
95. Hatakeyama J, Ono T, Takahashi M, Oda M and Shimizu H: Differentiating between primary central nervous system lymphoma and glioblastoma: The diagnostic value of combining ^{18}F-fluorodeoxyglucose positron emission tomography with arterial spin labeling. Neurol Med Chir (Tokyo) 61: 367-375, 2021.
96. Weller M, Martus P, Roth P, Thiel E and Korfel A; German PCNSL Study Group: Surgery for primary CNS lymphoma? Challenging a paradigm. Neuro Oncol 14: 1481-1484, 2012.
97. Deng X, Xu X, Lin D, Zhang X, Yu L, Sheng H, Yin B, Zhang N and Lin J: Real-World impact of surgical excision on overall survival in primary central nervous system lymphoma. Front Oncol 10: 131, 2020.
98. Labak CM, Holdhoff M, Bettegowda C, Gallia GL, Lim M, Weingart JD and Mukherjee D: Surgical resection for primary central nervous system lymphoma: A systematic review. World Neurosurg 126: e1436-e1448, 2019.
99. Schellekes N, Barbotti A, Abramov Y, Sitt R, Di Meco F, Ram Z and Grossman R: Resection of primary central nervous system lymphoma: Impact of patient selection on overall survival. J Neurosurg: Feb 26, 2021 (Epub ahead of print).
100. Bierman PJ: Surgery for primary central nervous system lymphoma: Is it time for reevaluation? Oncology (Williston Park) 28: 632-637, 2014.